Research Article

Jianzhang Huang, Shuang Gan, Yi Cai, Yijie Liu, and Yingjing Liang*

Molecular dynamics study on dynamic interlayer friction of graphene and its strain effect

https://doi.org/10.1515/ntrev-2023-0128
received June 6, 2023; accepted September 7, 2023

Abstract: This study delves into the mechanism of dynamic sliding friction between layers of graphene and its strain effect, through numerical analysis using molecular dynamics simulations. To eliminate the influence of commensurability and edge effect, a friction pair model with annular graphene as a slider is established. The research explores the quantifying effects of temperature, normal load, sliding velocity, support stiffness, and axial strain on the friction between graphene layers. The coupling effect of temperature and other influencing factors is also clarified. The results indicate that the interlayer friction increases with normal load by decreasing the interlayer spacing and increasing the atomic vibration amplitude. The ploughing phenomenon does not appear since the edge effect is eliminated by the model. Friction is initially enhanced at higher sliding velocities, but is later reduced by severe residual deformation and lattice resonance frequency. The support stiffness regulates interlayer friction by affecting the atomic vibration amplitude of the graphene lattice. Mechanism analysis shows that the number of effective contact atoms increases under axial strain, and the lattice vibration frequency is the main way to regulate the interlayer friction by strain effect. Our findings provide a fundamental understanding of the strains engineering of nanoscale friction and reveal the influence mechanism of affecting factors on the dynamic friction of graphene.

Keywords: dynamic interlayer friction, strain effects, lattice vibration, commensurability, graphene

*** Corresponding author: Yingjing Liang,** Department of Engineering Mechanics, School of Civil Engineering, Guangzhou University, Guangzhou, Guangdong 510006, China, e-mail: yjliang@gzhu.edu.cn
Jianzhang Huang, Shuang Gan, Yi Cai, Yijie Liu: Department of Engineering Mechanics, School of Civil Engineering, Guangzhou University, Guangzhou, Guangdong 510006, China

1 Introduction

Graphene is currently a highly researched topic in the nanomechanics field due to its exceptional mechanical, thermal, and electrical properties [1–4]. It has become a crucial main component of nanoelectromechanical system due to its remarkable physical properties including ultra-low interlayer friction [5,6]. Additionally, it is proposed to enhance the tribological and wear resistance properties of solid materials by incorporating nanomaterials during the manufacturing process. According to the research conducted by Gao *et al.*, adding 10 Vol% of alumina nanoparticles to Al/Al_2O_3 composites improves their wear resistance properties [7]. Over the past two decades, diamond-like carbon (DLC) films have attracted extensive research attention owing to their extraordinary tribological properties, making them a promising candidate for tribological modification of solid surfaces [8]. Even though DLC films have a low coefficient of friction and maintain a stable microstructure at high temperatures, their wear consumption is a crucial factor affecting their protection lifespan [9]. To increase the storage capacity of mechanical hard disks, Zhang *et al.* suggested using graphene as a key component instead of DLC film to create ultra-lubricated mechanical hard disks [10]. However, the effect of high sliding speed on the dynamic friction of graphene is not yet clear. Studies have shown that rotating the upper layer of graphene at a certain angle to form an incommensurate registry with the substrate layer can significantly decrease interlayer friction and result in superlubrication [11]. However, the superlubrication phenomenon may not occur in specific cases, such as ultra-high load [12] or contact with the low support stiffness of the substrate surface [13]. Interfacial friction between graphene layers is influenced by multiple factors including interlayer spacing, commensurability, normal load, temperature, support stiffness, and relative sliding velocity [14–17]. Therefore, understanding the effect and influence mechanisms of these factors on interlayer friction is of significant academic and engineering value.

The relationship between normal load and nanoscale friction on graphene layers is complex and varies depending

on their contact commensurability [12,18,19]. When the contact is commensurate, an increase in normal load enhances interlayer friction. However, when the contact is incommensurate, a low normal load has little effect on interlayer friction. When the normal force is increased to a certain value, friction increases significantly due to the ploughing phenomenon between the slider boundary atoms and substrate surface under high load. The influence of normal load on interlayer friction is related to edge effect and contact commensurability [20]. The relative sliding velocity also affects the interlayer friction tremendously [21]. The degree to which atoms are hindered by potential barriers varies depending on the relative velocity in the case of incommensurate contact, as a result, the interlayer friction exhibits a complicated variation law with respect to relative velocity [22–25]. Previous theoretical studies using traditional slider-substrate friction model have also shown that the edge effect and contact commensurability have complex influences on interlayer friction [26]. Multiple factors are often coupled together, and the mechanism behind the phenomena still needs to be further explored and revealed.

According to studies, strain has a significant impact on the characteristics and behaviors of nanomaterials [27–30]. In particular, to fulfill the demands of engineering applications, strains applied to graphene meet certain engineering requirements [12]. Researchers have discovered that in-plane strain can alter the static frictional force between graphene and silica substrate [31–33]. Uniaxial tensile strain applied to graphene can reduce friction by reducing the number of atoms between the indenter and graphene [34]. Conversely, compressive strain can increase the friction coefficient of the graphene interlayer friction [35]. However, the friction force might rise dramatically under slight compressive strain, despite an increase in the number of atoms in the contact area [30]. The complex mechanism of the interfacial frictional strain effect is not solely dominated by the change in the number of atoms in the contact area [21,36,37]. Instead, the strain causes incommensurate contact at the graphene interface, leading to a reduction in interlayer friction [38]. The existing research works used the lattice mismatch theory to describe how uniaxial tensile/compressive strain affected the surface friction of graphene. From the perspective of energy dissipation, the strain effect has an inevitable impact on the lattice vibration, which then affects the interfacial dynamic friction at the nanoscale [39]. In the theoretical studies of strain effect utilizing slider-substrate friction model [40], commensurability and lattice vibration have a combined effect on the friction generated by strain, and even the edge effect is included [41]. So far, there have been few studies on the influence of strain effect on dynamic friction of graphene interface from the perspective of kinetic dissipation. The mechanism of strain effect on dynamic friction through altering the number of contact atoms and phonon density of state (DOS) has not been clarified. Therefore, more research on nanoscale dynamic friction should emphasize the comprehensive study of the mechanism of the strain effect, as it has great potential for tuning the interfacial friction at the nanoscale.

This study introduces a new friction pair model consisting of an annular graphene rotational slider and substrate. Its purpose is to eliminate the influences of contact commensurability and edge effects. Through molecular dynamics (MD) simulation, the effects of temperature, normal load, sliding velocity, support stiffness, and axial strain on the interfacial friction between graphene layers are investigated in this work. The numerical and theoretical analyses are performed to study the influence mechanism of these factors on friction. Additionally, the impacts of axial strain on interlayer friction are revealed by conducting statistical analysis of phonon DOSs and examining effective contact area between strained graphene layers.

2 Simulation model and methods

In the physical model of the rotational slider-substrate friction pair system shown in Figure 1, an annular-shaped graphene flake slider is placed on a rectangular graphene substrate with an equilibrium spacing of 0.34 nm. This annular model has both inner and outer edges that enhance its ability to resist out-of-plane deformation during rotation and allows for better control of rotation compared to a circular model. To simulate the supporting effect on the graphene substrate, a spring with a stiffness of 2.7 nN/nm is used to apply restoring force in the out-of-plane direction to the carbon atoms of graphene substrate [13,42,43]. The rectangular graphene substrate has dimensions of 10 nm in both length and width and contains 3,936 carbon atoms. By restricting the atomic mobility of 384 carbon atoms in total, a 2 Å wide area on all four sides of the graphene substrate are retained and fixed. The annular graphene slider with 1,427 atoms has an inner and outer radius of 2 and 3 nm, respectively. The area with width of 2 Å on the inner and outer edges of annular graphene is fixed. The interlayer friction is calculated using the steady isothermal method, which records the thermal energy in the simulation process. The edge effect on nanoscale friction mainly occurs when the slip flake slides along the normal direction of the edge [44]. Using the graphene friction pair model proposed in this work, all the boundary atoms move in the tangential direction of the edge during rotation. Therefore, although the

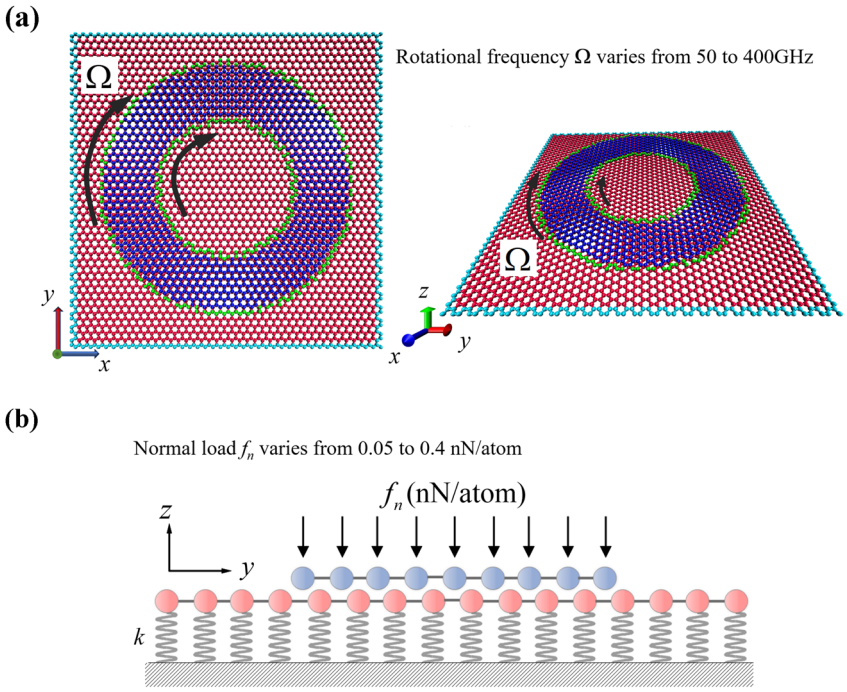

Figure 1: Schematic of the friction pair model: (a) Physical model of rotational slider-substrate friction pair system. The substrate has dimensions of 10 nm in both length and width and the upper layers of graphene have an inner ring radius of 2 nm and an outer ring radius of 3.7 nm. (b) Each of the substrate graphene atoms is linked to a linear spring in the *z*-direction. The normal load f_n varying from 0.05 to 0.4 nN/atom is applied on each of the annular graphene flake atoms.

edge area is increased, the edge effect in the process of friction can be eliminated. During the rotation process, the crystal lattice mismatch of the contact interface is constantly updated, and the atoms in the contact area are stressed uniformly to effectively avoid the influence of commensurability effects and edge effects.

In this study, the chiral edges of the graphene model are identified as armchair in the *y* direction and zigzag in the *x* direction. The impact of uniaxial strain on friction force is analyzed in relation to these two different chiral types of edges. To apply the strain, the atoms in the loading edges are displaced gradually along the uniaxial direction by 0.02 Å every 0.01 ns. Prior to strain application, the simulation system undergoes a 0.2 ns relaxation to reach equilibration. Similarly, after the strain loading is complete, another 0.2 ns relaxation period is conducted to ensure system equilibration before relative sliding simulation. Figure 2 shows a schematic representation of uniaxial strain loading on zigzag graphene. The uniaxial strain is applied to the green area after the system has attained stability and is calculated using the formula: $\varepsilon = (L - L_0)/L_0$, where the L and L_0 are the side length of substrate graphene in the loading direction before and after deformation, respectively.

The dynamic friction process between graphene layers is simulated using a large-scale atomic/molecular massively parallel simulator package. The simulation system is set to a non-periodic boundary condition along the *x*, *y*, and *z* directions, and the dimensions of the simulation box are 40 × 40 × 10 nm^3 (length × width × height). The carbon atoms on the edges of the substrate graphene are fixed. The remaining atoms on substrate graphene are attached to a spring along *z*-axis to simulate the supporting effect on the substrate. The normal load of 0.10 nN/atom (*z*-oriented) is imposed on each carbon atom of the upper graphene. The AIREBO potential [45] is used to describe the interlayer C–C bond interaction of graphene.

The upper annular graphene is simulated under an NVE ensemble, and the substrate graphene is simulated under an NVT ensemble to extract the energy consumed by friction. The time step is set to 1 fs for all simulations. Energy minimization is performed at the beginning of the simulations to achieve equilibrium. After the system relaxation of 0.2 ns, the upper annular graphene rotates at high speed around its central axis in the *z*-direction to simulate the dynamic interlayer sliding behavior. The heat generated by interlayer friction is recorded by using a Nosé–Hoover thermostat after the system is sufficiently relaxed to reach the stability of high-speed rotation. The time of the rotation process is 2 ns. The interlayer friction force of each atom is calculated by using the steady

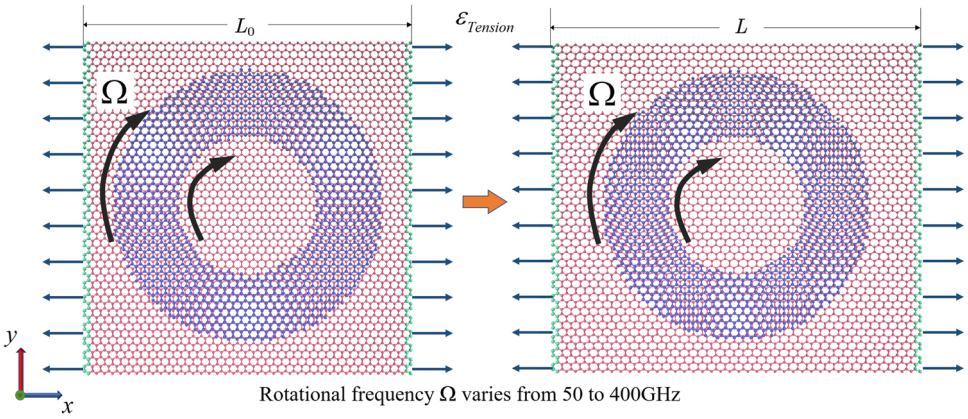

Figure 2: Schematic of substrate graphene subjected to uniaxial strains. The uniaxial strain is applied to the green area and calculated as follows: $\varepsilon = (L - L_0)/L_0$, where the distance after the stretch is L, and the distance before the stretch is L_0.

isothermal method [46]. The energy dissipation rate by friction is computed using the energy data extracted by the Nosé–Hoover thermostat as follows:

$$\Delta E = \int_0^t Q' \mathrm{d}t,$$

where Q' is the energy dissipation rate and ΔE is the thermal energy produced by dynamic friction. Thus, the friction between the layers is calculated as follows:

$$F_f = \frac{Q'}{2\pi f R},$$

where f is the rotational frequency of the upper layer, and R is the rotational radius of the upper circle.

Friction is the conversion of phonons by the sliding motion between contact surfaces [47,48]. To analyze energy exchange across the graphene interfaces from a vibration perspective, the DOS is calculated as follows [49]:

$$\mathrm{DOS}(\omega) = \frac{1}{\sqrt{2\pi}} \int_0^\tau e^{i\omega t} \frac{\langle v(t) \cdot v(0) \rangle}{\langle v(0) \cdot v(0) \rangle} \mathrm{d}t,$$

where ω is the frequency, $v(t)$ is the velocity of each atom at time t, τ is the rotational time of 2 ns, < > denotes the ensemble average and is calculated as follows [50]:

$$\langle v(t) \cdot v(0) \rangle = \frac{1}{M} \sum_{j=1}^{M} \frac{1}{N} \sum_{i=1}^{N} v_{j,i} \cdot v_{j,i+\frac{t}{\Delta t}},$$

where M is the number of atoms in the effective contact area, and $v_{j,i}$ denote the velocity of atom j at time step i. Velocities in DOS are calculated from an equilibrium NVT ensemble for 10 fs.

3 Results and discussion

3.1 Normal load effects

The upper annular graphene rotates at a frequency of 150 GHz, and the average relative speed of the annular graphene's inner and outer edges is 29.6 Å/ps. The substrate graphene layer's supporting spring stiffness is 2.7 nN/nm. Temperature dependence of normal load effects is being studied, with environmental temperature ranging from 100 to 500 K. Figure 3 illustrates the variation in the normal load applied to each atom of the upper annular graphene, ranging from 0.05 to 0.4 nN/atom.

The calculation results of interlayer friction under various normal loads are displayed in Figure 4. It is evident

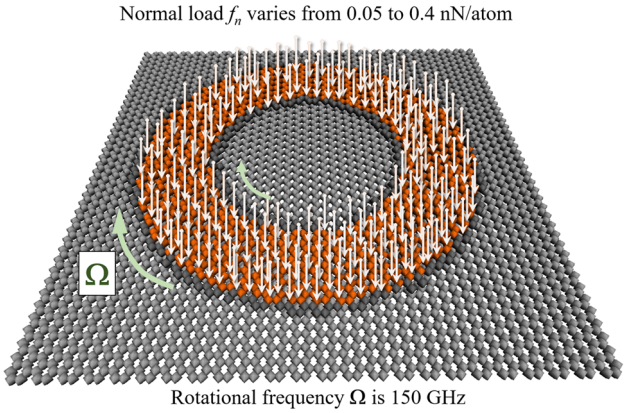

Figure 3: Schematic of annular graphene subjected to normal load: each atom of the annular graphene in the orange region is subjected to normal load f_n, where the rotational frequency is 150 GHz.

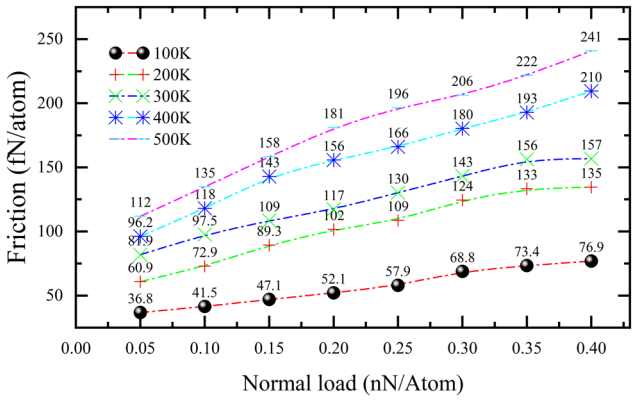

Figure 4: The effects of normal load on the interfacial friction of graphene under different temperatures.

that the normal load has a significant impact on friction. The interlayer distance and the atomic lattice vibration amplitude of substrate graphene are shown in Table 1 and Figure 5. As the distance between the annular and substrate graphene decreases and the atomic lattice vibration amplitude rises, interlayer friction increases linearly with the normal loads at the same temperature. It is observed from the approximate linear increase in friction with normal load that the ploughing phenomenon does not appear. The ploughing phenomenon usually occurs when the slip flake slides along the normal direction of the edge. When the normal load is too large, the bottom substrate is squeezed and produces excessive deformation, resulting in a sharp rise in the friction force during sliding. Therefore, the ploughing phenomenon is often accompanied by edge effects. In the friction pair model proposed in this work, the relative sliding direction is the tangential direction of the edge. Consequently, there is no ploughing phenomenon as the normal load rises.

Moreover, the atomic vibrational frequency of graphene lattice increases with the increase in temperature [51], as well as the atomic vibrational amplitude as shown in Figure 6. The friction force also rises with temperature due to a higher atomic lattice vibration frequency and amplitude, which strengthens the interlayer atomic interaction. Under lower temperatures, the atomic lattice vibration frequency and amplitude are relatively low, making it easier for the atoms of rapidly rotating annular graphene to pass through the energy barrier on the substrate graphene surface. This reduces energy dissipation during relative sliding. Through the annular rotating friction model that eliminates commensurability and edge effects, these results demonstrate that interlayer friction increases with normal load and temperature. It implies that interlayer friction is positively correlated with normal load and temperature. Therefore, it is reasonable to conclude that interlayer friction is positively correlated with normal load and ambient temperature.

Table 1: Variation in interlayer distance with normal load

Normal load (nN/atom)	0.05	0.1	0.15	0.2	0.25	0.3	0.35	0.4
Interlayer distance (Å)	2.368	2.286	2.189	2.094	2.002	1.910	1.834	1.765

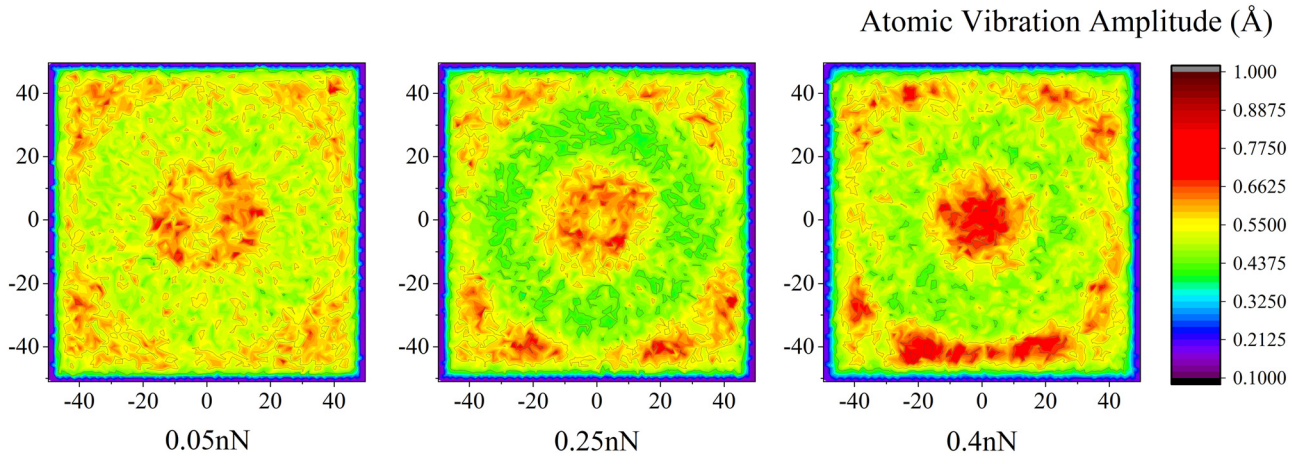

Figure 5: The nephogram of atomic out-of-plane vibration amplitude of the substrate graphene under different normal loads when temperature T = 300 K.

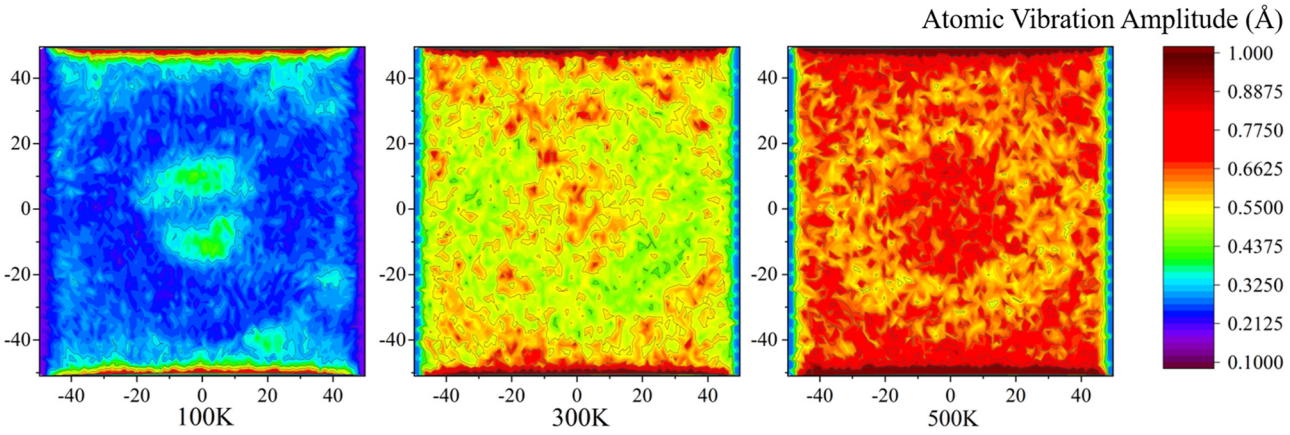

Figure 6: The nephogram of atomic out-of-plane vibration amplitude of the substrate graphene at different temperatures when the normal load is 0.1 nN/atom.

The relative coefficient parameter α is defined to investigate the coupling influence of temperature and normal load on the interlayer friction as follows [52]:

$$\alpha = \frac{F_{0.4\text{nN}} - F_{0.05\text{nN}}}{F_{0.05\text{nN}}},$$

where the $F_{0.4\text{nN}}$ and $F_{0.05\text{nN}}$ represent the friction force when the normal load is 0.4 nN/atom and 0.05 nN/atom, respectively. Table 2 displays the different values of α at varying temperatures. The interlayer friction nearly doubles when the normal load increases from 0.05 to 0.4 nN/atom at all temperatures. The interlayer friction increases by a comparatively modest 91.69% at room temperature (300 K). When the temperatures are 200 and 400 K, which are close to room temperature, the rate of interlayer friction increases considerably more quickly than it does at 300 K. This rate is 118.29% at 200 K and 121.67% at 400 K, respectively. Moreover, at 100 K, it increases by 115.17%, and at 500 K, it increases by 108.96%. This indicates that temperature plays a crucial role in the amplifying efficiency of normal load effects on friction.

3.2 Rotational frequency effects

The annular graphene is subjected to a normal load of 0.1 nN/atom, while the substrate graphene has a supporting stiffness of 2.7 nN/nm. The rotational frequency of the annular graphene varies from 50 to 400 GHz at the same temperature, with an average relative velocity of 9.87–78.94 Å/ps between the inner and outer edges of the annular graphene. Figure 7 illustrates the calculation results. At 300 K, the interlayer friction increases with the rotational frequency until 300 GHz, beyond which it decreases. At 300 GHz, the interlayer friction value reaches its maximum of 182.68 fN/atom. The rotational frequency that induces the maximum value of interlayer friction increases as the temperature rises. This phenomenon is brought on by both the in-plane deformation of graphene brought on by interlayer friction and the velocity-coupled thermally induced resonance of the graphene lattice. The interlayer lattice vibration frequency and

Table 2: Parameters α under different temperatures

Temperature (K)	100	200	300	400	500
α (%)	115.17	118.29	91.69	121.67	108.96

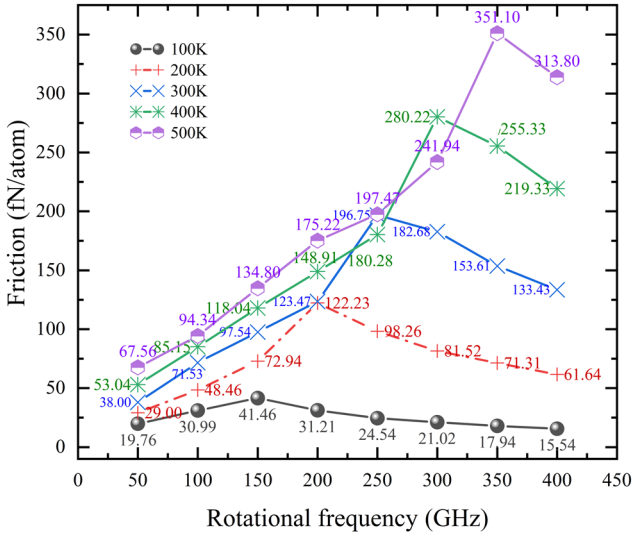

Figure 7: Effects of rotational frequency on the interfacial friction of graphene under different temperature.

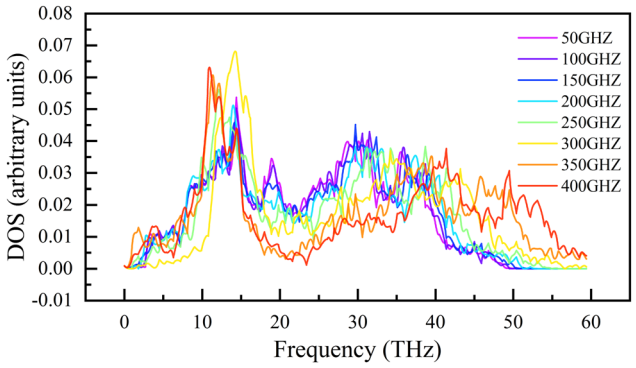

Figure 8: Phonon state density distribution at different rotational frequencies when the normal load is 0.1 nN/atom and the temperature is 300 K.

in-plane deformation of substrate graphene at 300 K are calculated to explain the effect of the rotational frequency on interlayer friction. As shown in Figure 8, the density of phonon moves toward the high frequency region with the increase in rotational frequency. As a result, the more intense interlayer vibration leads to increased energy exchange, which increases the interlayer friction. However, when the rotational frequency is increased to 300 GHz, the density of phonon peak in the frequency range of 10–35 THz increases sharply. And as the rotational frequency continues to increase, this density peak shifts toward the low frequency, resulting in a decrease in energy conversion efficiency, and therefore a decrease in friction. In addition, the average in-plane atomic displacement of the substrate graphene at 50, 200, and 400 GHz rotational frequency are calculated to reflect the in-plane deformation of the substrate graphene [53], as shown in Figure 9. The results show that the in-plane deformation near the interlayer contact area of the substrate graphene accumulates and intensifies with the increase in the rotational frequency.

The interlayer lattice resonance vibration becomes more intense when the relative sliding velocity approaches the lattice resonance frequency of the graphene interface, resulting in extensive energy dissipation and maximum interlayer friction [53]. The frequency of graphene's interlayer lattice resonance rises with temperature, which also raises the rotational frequency necessary to generate lattice resonance. However, throughout the interlayer sliding process, graphene's elastic deformation encounters accumulation and release [54]. The friction-induced deformation mechanism significantly affects interlayer friction at low temperatures. While at high temperatures, the energy dissipation mechanism of thermal-induced resonance dominates, increasing the rotational frequency required for interlayer lattice resonance. When the rotational frequency is higher than a certain key value, the interlayer friction-induced deformation energy is difficult to entirely release, which causes cumulative deformation and a change in the lattice constant of graphene. As a result, the interlayer friction is decreased along with the interlayer lattice mismatch caused by the variance in in-plane lattice constant between the graphene layers.

The interlayer friction tends to increase with temperature at the same rotational frequency. However, when the rotational frequency is 300 GHz, the interlayer friction force is higher at 400 K than it is at 500 K. This is due to the interlayer lattice resonance phenomenon induced by the combined effects of rotational frequency and temperature, which dramatically amplifies the friction force. Figure 7 shows that at a temperature of 300 K, the interlayer friction at 350 GHz is about five times greater than that at 50 GHz. Therefore, eliminating lattice resonance effectively reduces

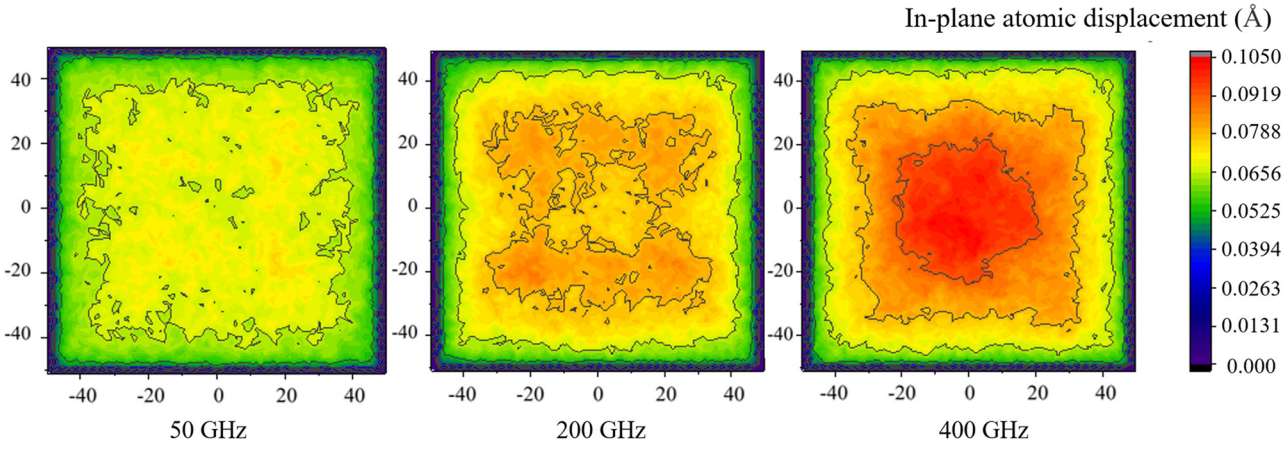

Figure 9: The in-plane deformation of substrate graphene at different rotational frequencies when the normal load is 0.1 nN/atom and the temperature is 300 K.

friction dissipation, making it a potential technique for nanoscale friction regulation.

3.3 Supporting stiffness effects

In practical applications, graphene is typically deposited on the substrate or appears as several layers. The supporting effect becomes one of the key factors affecting the graphene's interlayer friction since the interaction between graphene and substrate differs depending on substrate materials [13,40,42]. To evaluate the effects of support on graphene interlayer friction, the supporting stiffness is set to range from 1 to 15 nN/nm at the same temperature. The calculation results are displayed in Figure 10. It is discovered that a maximum value of interlayer friction occurs with an increase in support stiffness at all temperatures, and their corresponding value of supporting stiffness falls in the range of 3–5 nN/nm. As the supporting stiffness increases, the interlayer friction reduces after the maximum value is reached.

This is due to the fact that when the supporting stiffness is low, the substrate graphene is weakly restricted in the out-of-plane direction, making it easy for the substrate graphene to produce out-of-plane deformation when it gets pressed by the annular graphene. Consequently, there is a relatively wide equilibrium spacing between the graphene layers and low interlayer friction. With an increase in supporting stiffness, the substrate graphene's resistance to out-of-plane deformation has improved and the equilibrium spacing between graphene layers is decreased. As a result, the interaction between the annular and substrate graphene is stimulated, triggering the interlayer friction to gradually rise. Meanwhile, from the perspective of lattice dynamics, the lattice vibration frequency of the graphene substrate increases with supporting stiffness [13,42], raising the peak of the interlayer potential barrier. This enhances the energy dissipation throughout the friction process and leads to an increase in the interlayer friction.

However, as the supporting stiffness continues to increase, the vibration amplitude of the substrate graphene lattice becomes limited, and the interlayer interaction between the graphene layers is reduced. In consequence of this, the annular graphene layer may more easily pass through the substrate graphene surface's potential barrier, thereby lowering energy dissipation during the sliding process. It presents a gradual decrease in friction with the increase in the supporting stiffness. As can be observed in Figure 10(e), at a temperature of 100 K, there is no peak value of friction as the supporting stiffness increases. This is attributed to the weakening of the lattice vibration's thermal excitation effect, and the lowered frequency and amplitude of graphene lattice vibration at low temperatures. It is attributed to the lower frequency and amplitude of graphene lattice vibration at low temperatures, and the thermal excitation effect of lattice vibration is weakened. Hence, the inhibition effect on lattice vibration increases as the supporting stiffness increases, resulting in a decreasing trend of interlayer friction.

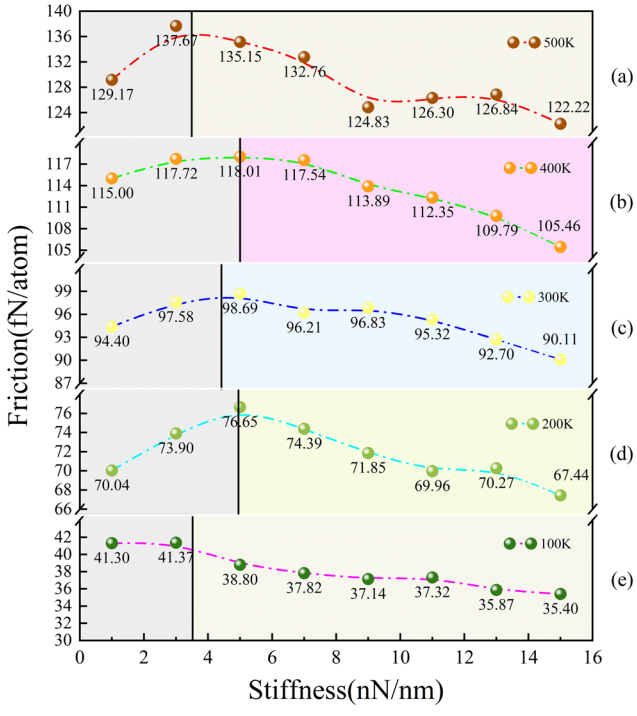

Figure 10: The effect of support stiffness on the interfacial friction of graphene under different temperatures. (a) 500 K, (b) 400 K, (c) 300 K, (d) 200 K, (e) 100 K.

3.4 Uniaxial strain effects

We conducted a study on the impact of uniaxial strain along the chiral edge type on interlayer friction. The chiral armchair or zigzag type in our results refers to the loading direction of uniaxial strains. Figure 11 depicts the calculated results of the interlayer friction under varying uniaxial strains. Our findings indicate that the friction of graphene reduces with the increase in tensile strain. Specifically, the interlayer friction of armchair graphene drops by 15.96% and that of zigzag graphene drops by 16.27% when the tensile strain is 10%. In contrast, interlayer friction increases as compressive strain increases when the uniaxial compressive strain is less than −3%. However, when the

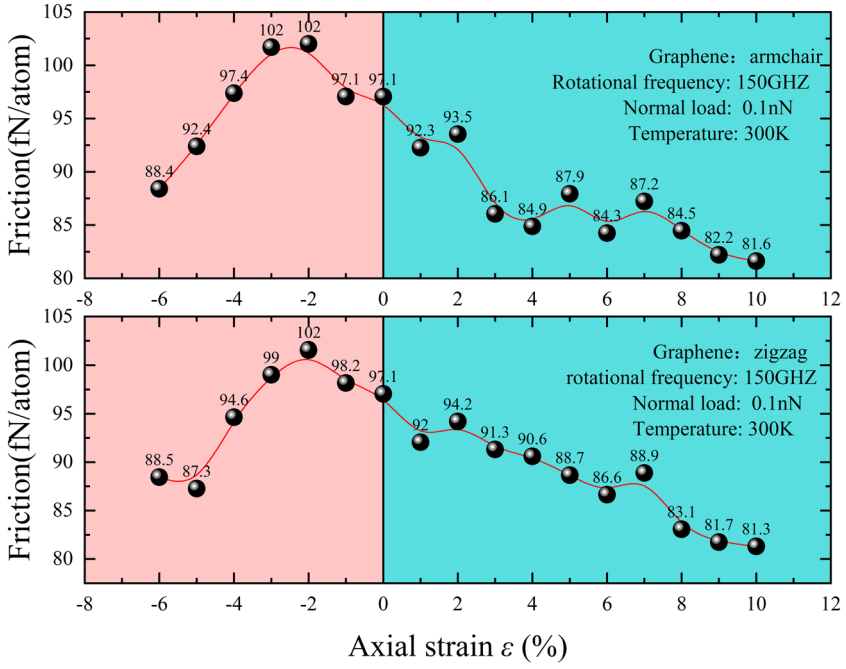

Figure 11: Effect of uniaxial strain on the interfacial friction of graphene.

compressive strain exceeds −3%, the friction between graphene layers decreases as the compressive strain intensifies.

Altering the number of atoms in the contact area is considered to be one of the main ways that strain impacts the nanoscale interfacial friction. When subjected to uniaxial strain, the graphene friction pair's effective contact area is affected, changing the number of atoms in the contact region. As illustrated in Figure 12, the number of atoms in the contact region increases from 1,435 to 1,538 as the tensile strain rises. Because the atoms in the non-contact region of the substrate graphene below the inner circle space of the annular graphene move into the sliding contact region. Furthermore, the Poisson effect causes a number of atoms to enter the contact region from the lateral direction. Although, a small number of atoms in substrate graphene initially close to the outer circle edge of annular graphene migrate out of the contact region during uniaxial tensile deformation, the number of effective contact atoms increases as the number of atoms entering the contact region is always more than those migrating out of the contact region. Therefore, the number of atoms in the contact region increases with the tensile strain. On the other hand, during compression strain, the atoms near the contact boundary move into the contact region, causing an increase in the number of atoms to 1,672. It was proposed that the tensile strain reduced friction by decreasing the number of atoms in effective contact. However, the results imply that although the number of effective contact atoms plays a role in interlayer friction, it is not the main factor of strain effect on nanoscale interfacial friction. Under tensile strain, the potential barrier amplitude on the substrate graphene's surface decreases, making it easier for atoms in annular graphene to slide through the substrate graphene's surface, resulting in reduced energy dissipation of interlayer friction behavior.

In our analysis, an effective contact area on the substrate is selected for calculating the DOS of graphene during the friction process. The phonon spectra of graphene under the uniaxial strain effect are calculated, as illustrated in Figure 13. The phonon density peak at around

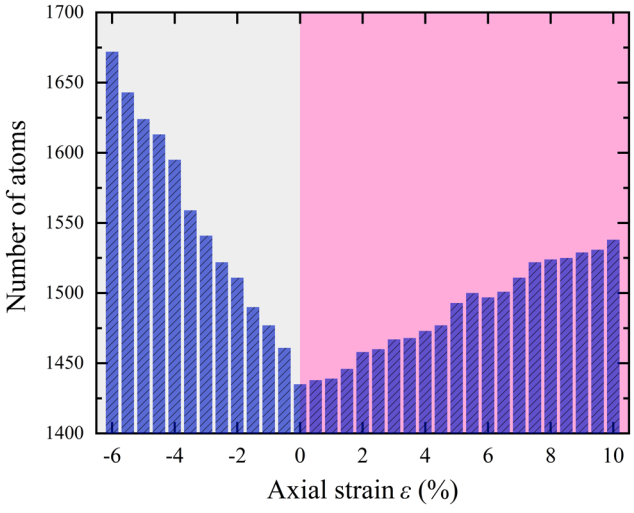

Figure 12: Number of effective contact atoms of graphene under uniaxial strain.

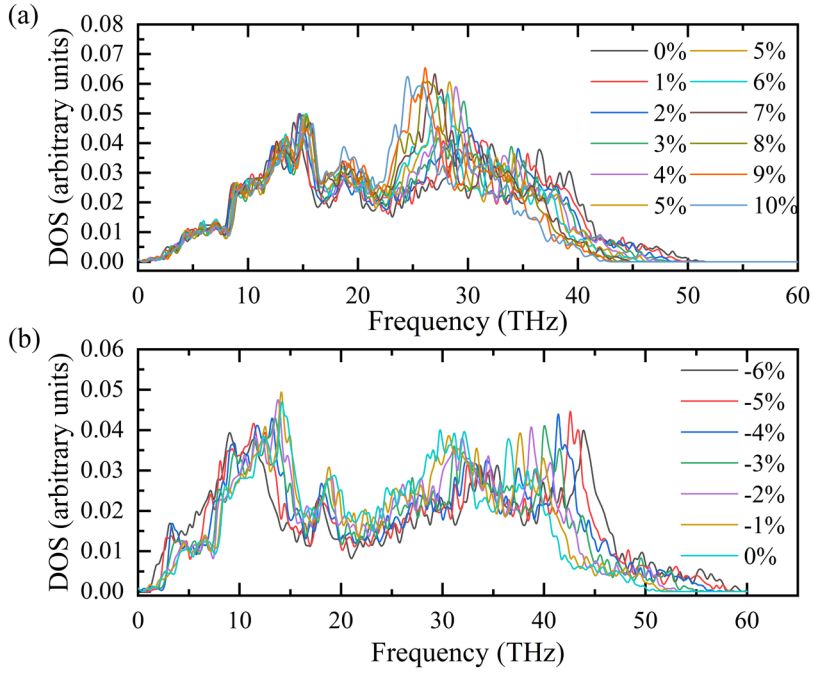

Figure 13: Phonon state density of graphene under uniaxial strain: (a) tensile strain and (b) compressive strain.

28 THz shifts to the low frequency as the uniaxial strain increases, where it is at around 25 THz when the tensile strain is 10%. It demonstrates that the interlayer lattice atomic interaction is weakened by the uniaxial tensile strain, which causes the phonon energy to be in a comparatively low energy state and increases the number of low-frequency phonons. The energy exchange in the friction process is decreased by a large number of low-frequency phonons, making it difficult for the ordered kinetic energy to dissipate effectively and therefore reducing the interlayer friction.

In Figure 12, it can be observed that there is an increase in the number of effective contact atoms when a slight compressive strain is applied. Under modest compression, the

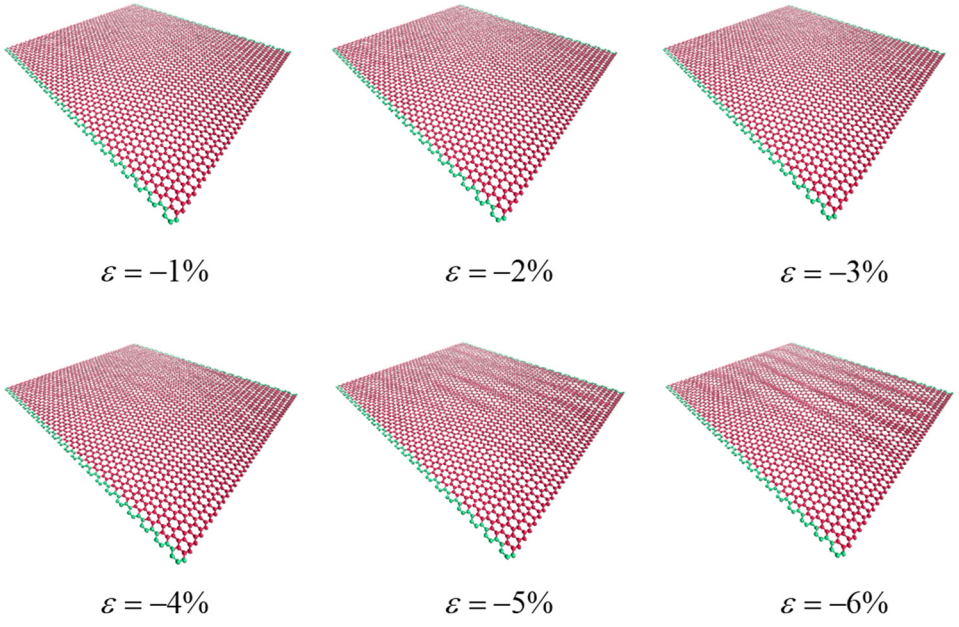

Figure 14: Formation process of the wrinkles in the substrate graphene under compressive strain loading.

interatomic interaction within the substrate graphene is enhanced, leading to an increase in the potential barrier on the substrate graphene surface. As a result, more energy is required to overcome this potential barrier during interlayer sliding, which ultimately increases the interlayer friction. The phonon spectra of the compressed graphene, as shown in Figure 13(b), demonstrate that the phonon spectral peak moves toward higher frequencies with the increase in compressive strain. This shift in the high-frequency phonons facilitates the efficiency of energy exchange, thus increasing interlayer friction. However, when the uniaxial compressive strain is more than −3%, the friction reduces as the uniaxial compressive strain increases. This decrease can be attributed to the formation of wrinkles in the substrate graphene under high compressive strain, as illustrated in Figure 14. Local ripples have appeared in the substrate graphene when the compression strain reaches −4%, and then the global wrinkles become manifest when the compression strain is −6%. These wrinkles reduce the interfacial effective contact area between the substrate and the annular graphene, which in turn affects the vibration amplitude and frequency of the substrate graphene lattice. The decrease in interlayer interaction ultimately results in a decrease in friction.

4 Conclusion

This study proposes a new model to eliminate commensurability and edge effects and studies the effects of environmental variables and strain effect on friction to reveal their influence mechanism using MD. It is discovered that after the boundary effect is eliminated, the friction between layers increases linearly with the normal load, and the ploughing phenomenon is suppressed. However, the friction between layers varies nonlinearly with relative velocity. The graphene lattice resonates under the influence of thermal effect and sliding velocity, leading to maximum friction at a specific rotational frequency. The frequency of thermal-induced lattice resonance increases with temperature, resulting in an increase in the rotational frequency that causes the maximum friction. Supporting stiffness decreases interlayer friction by improving the resistance of substrate graphene to out-of-plane deformation while limiting the lattice vibration amplitude of the substrate, that makes it easier for slider graphene to overcome the potential barrier of the substrate graphene surface and reducing energy dissipation during interlayer sliding. Tensile strain efficiently reduces friction, and this reduction is not primarily due to the change in the number of effective contact atoms. While slight compressive strain increases the interlayer friction. However, wrinkles emerge on the substrate graphene when the compressive strain exceeds −3%, weakening the interlayer atomic interaction and decreasing friction. The phonon spectrum analysis shows that altering the phonon energy distribution and interlayer energy exchange efficiency is the main way for axial strain to regulate the interlayer friction. The findings from this study provide a theoretical basis for the regulation of nano-dynamic friction. Some strategies can be adopted to reduce the nanoscale interface friction, such as avoiding the boundary effect and velocity-temperature lattice resonance as far as possible, and selecting the substrate with stiff elastic stiffness as the support of the friction surface. At the same time, if possible, a slight tensile strain can be applied to reduce the interface friction. The research works in this study are expected to provide theoretical guidance for regulating nanoscale friction and implementing its strain engineering.

Funding information: The authors wish to acknowledge the support from the National Nature Science Foundation of China (Grant No. 12102097, 12002094, and 52178193), Natural Science Foundation of Guangdong Province (Grant No. 2020A1515010915, 2022A1515012037, 2018A030310310, and 2022A1515012086), Guangzhou Municipal Science and Technology Project (Grant No. 202102021026 and 202102020606).

Author contributions: All authors have accepted responsibility for the entire content of this manuscript and approved its submission.

Conflict of interest: The authors state no conflict of interest.

References

[1] Wu X, Han Q. Thermal conductivity of defective graphene: an efficient molecular dynamics study based on graphics processing units. Nanotechnology. 2020;31(21):215708.
[2] Wu X, Han Q. Phonon thermal transport across multilayer graphene/hexagonal boron nitride van der waals heterostructures. ACS Appl Mater Interfaces. 2021;13(27):32564–78.
[3] Guo W, Bai Q, Dou Y, Chen S, Wang H. Molecular dynamics simulation of frictional strengthening behavior of graphene on stainless steel substrate. Carbon. 2022;197:183–91.
[4] Li C, Tang W, Tang X-Z, Yang L, Bai L. A molecular dynamics study on the synergistic lubrication mechanisms of graphene/water-based lubricant systems. Tribol Int. 2022;167:107356.
[5] Fennimore AM, Yuzvinsky TD, Han WQ, Fuhrer MS, Cumings J, Zettl A. Rotational actuators based on carbon nanotubes. Nature. 2003;424(6947):408–10.

[6] Zhou M, Zhou C, Luo K, Li W, Liu J, Liu Z, et al. Ultrawide bandwidth and sensitive electro-optic modulator based on a graphene nanoelectromechanical system with superlubricity. Carbon. 2021;176:228–34.
[7] Gao Y, Vini MH, Daneshmand S. Effect of nano Al_2O_3 particles on the mechanical and wear properties of Al/Al_2O_3 composites manufactured via ARB. Rev Adv Mater Sci. 2022;61(1):734–43.
[8] Liu JQ, Yang T, Cao HT, Deng QY, Pan CJ, Wen F. Diamond-like carbon films for tribological modification of rubber. Nanotechnol Rev. 2022;11(1):2839–56.
[9] Zeng Q, Ning Z. High-temperature tribological properties of diamond-like carbon films: A review. Rev Adv Mater Sci. 2021;60(1):276–92.
[10] Zhang S-M, Vu C-C, Li Q-Y, Tagawa N, Zheng Q-S, editors. Superlubricity relevant in hard disk drive applications. ASME Conference on Information Storage and Processing Systems. Santa Clara, CA: ASME; 2016 Jun 20–21.
[11] Li J, Peng Y, Tang X, Xu Q, Bai L. Effect of strain engineering on superlubricity in a double-walled carbon nanotube. Phys Chem Chem Phys. 2021;23(8):4988–5000.
[12] van Wijk MM, Dienwiebel M, Frenken JWM, Fasolino A. Superlubric to stick-slip sliding of incommensurate graphene flakes on graphite. Phys Rev B. 2013;88(23):235423.
[13] Zhang H, Guo Z, Gao H, Chang T. Stiffness-dependent interlayer friction of graphene. Carbon. 2015;94:60–6.
[14] Ru G, Qi W, Tang K, Wei Y, Xue T. Interlayer friction and superlubricity in bilayer graphene and MoS_2/$MoSe_2$ van der Waals heterostructures. Tribol Int. 2020;151:106483.
[15] Dhanola A, Khanna N, Gajrani KK. A critical review on liquid superlubricitive technology for attaining ultra-low friction. Renew Sustain Energy Rev. 2022;165:112626.
[16] Shen Y, Lei W, Tang W, Ouyang T, Liang L, Tian ZQ, et al. Synergistic friction-reduction and wear-resistance mechanism of 3D graphene and SiO2 nanoblend at harsh friction interface. Wear. 2022;488–9:204175.
[17] Torkaman-Asadi MA, Kouchakzadeh MA. Atomistic simulations of mechanical properties and fracture of graphene: A review. Comput Mater Sci. 2022;210:111457.
[18] Guo W, Yin J, Qiu H, Guo Y, Wu H, Xue M. Friction of low-dimensional nanomaterial systems. Friction. 2014;2(3):209–25.
[19] Lin K, Li D, Ye Y, Ye Z, Jiang W, Qin QH, et al. Friction behavior of 2D hydrogenated diamond-like films and bilayer graphene. Diam Relat Mater. 2022;127:109179.
[20] Huang Z, Chen S, Lin Q, Ji Z, Gong P, Sun Z, et al. The mechanisms of friction enhancements on graphene surfaces with folds: The reinforcement of atomic pinning or attraction. Tribol Int. 2022;165:107297.
[21] Li S, Li Q, Carpick RW, Gumbsch P, Liu XZ, Ding X, et al. The evolving quality of frictional contact with graphene. Nature. 2016;539(7630):541.
[22] Hayashi K, Tanaka D, Maruyama T, Araki H, Matsumura D, Kaneko M. Velocity-dependent threshold behavior of wearless nano-friction as studied in terms of spatial distribution of the local quasi-temperature. Comput Phys Commun. 2008;179(1–3):98–101.
[23] Hayashi K, Shiraishi T, Toyoda K, Tanaka F, Mori T, Hata T. Temperature-controlled molecular dynamics study on velocity-dependent threshold behavior of dynamic nano-friction. Comput Phys Commun. 2011;182(9):2032–5.
[24] Müser MH. Velocity dependence of kinetic friction in the Prandtl-Tomlinson model. Phys Rev B. 2011;84(12):125419.
[25] Ouyang T, Shen Y, Lei W, Xu X, Liang L, Waqar HS, et al. Reduced friction and wear enabled by arc-discharge method-prepared 3D graphene as oil additive under variable loads and speeds. Wear. 2020;462:203495.
[26] Nian J, Si Y, Guo Z. Advances in atomic-scale tribological mechanisms of solid interfaces. Tribol Int. 2016;94:1–13.
[27] Spear JC, Ewers BW, Batteas JD. 2D-nanomaterials for controlling friction and wear at interfaces. Nano Today. 2015;10(3):301–14.
[28] Wang X, Tantiwanichapan K, Christopher JW, Paiella R, Swan AK. Uniaxial strain redistribution in corrugated graphene: clamping, sliding, friction, and 2D band splitting. Nano Lett. 2015;15(9):5969–75.
[29] Lee JH, Lee S, Jeon JH, Oh DY, Shin M, Lee MJ, et al. Universality of strain-induced anisotropic friction domains on 2D materials. NPG Asia Mater. 2018;10:1069–75.
[30] Wang K, Qu C, Wang J, Ouyang W, Ma M, Zheng Q. Strain engineering modulates graphene interlayer friction by moire pattern evolution. ACS Appl Mater Interfaces. 2019;11(39):36169–76.
[31] Kitt AL, Qi Z, Remi S, Park HS, Swan AK, Goldberg BB. How graphene slides: measurement and theory of strain-dependent frictional forces between graphene and SiO_2. Nano Lett. 2013;13(6):2605–10.
[32] Huang J, Han Q. Mechanism of axial strain effects on friction in carbon nanotube rotating bearings. Nanotechnology. 2018;29(32):325703.
[33] Peng Y, Li J, Tang X, Liu B, Chen X, Bai L. Friction reduction of hydrogenated graphene by strain engineering. Tribol Lett. 2020;68(1):22.
[34] Bai Q, He X, Bai J, Tong Z. An atomistic investigation of the effect of strain on frictional properties of suspended graphene. AIP Adv. 2016;6(5):055308.
[35] Yang L, Guo Y, Zhang Q. Frictional behavior of strained multilayer graphene: Tuning the atomic scale contact area. Diam Relat Mater. 2017;73:273–7.
[36] Huang J, Han Q. Study on wrinkling in graphene under gradient shear by molecular dynamics simulation. J Mol Model. 2015;21(2):1–8.
[37] Huang J, Han Q. Strain effects on rotational property in nanoscale rotation system. Sci Rep. 2018;8:432.
[38] Guerra R, van Wijk M, Vanossi A, Fasolino A, Tosatti E. Graphene on h-BN: to align or not to align? Nanoscale. 2017;9(25):8799–804.
[39] Jiang J-W, Leng J, Li J, Guo Z, Chang T, Guo X, et al. Twin graphene: A novel two-dimensional semiconducting carbon allotrope. Carbon. 2017;118:370–5.
[40] Lin X, Zhang H, Guo Z, Chang T. Strain engineering of friction between graphene layers. Tribol Int. 2019;131:686–93.
[41] Yang X, Wang W. Friction characteristics in graphene/MoS_2 heterojunction. Surf Sci. 2023;728:122207.
[42] Li J, Peng Y, Tang X, Yang Z, Chen C, Bai L. Load-oriented thickness-dependent friction behavior of graphene supported by substrate with different stiffnesses. Comput Mater Sci. 2022;203:111164.
[43] Liao Y, Li Z, Nie W, Xia W. Effect of reconstructed vacancy defects on the crumpling behavior of graphene sheets. Forces Mech. 2022;6:100057.
[44] Zhang H, Chang T. Edge orientation dependent nanoscale friction. Nanoscale. 2018;10(5):2447–53.
[45] Orekhov N, Ostroumova G, Stegailov V. High temperature pure carbon nanoparticle formation: Validation of AIREBO and ReaxFF reactive molecular dynamics. Carbon. 2020;170:606–20.

[46] Cook EH, Buehler MJ, Spakovszky ZS. Mechanism of friction in rotating carbon nanotube bearings. J Mech Phys Solids. 2013;61(2):652–73.
[47] Liu X-Z, Ye Z, Dong Y, Egberts P, Carpick RW, Martini A. Dynamics of atomic stick-slip friction examined with atomic force microscopy and atomistic simulations at overlapping speeds. Phys Rev Lett. 2015;114(14):146102.
[48] Dong Y, Tao Y, Feng R, Zhang Y, Duan Z, Cao H. Phonon dissipation in friction with commensurate-incommensurate transition between graphene membranes. Nanotechnology. 2020;31(28):285711.
[49] Luo T, Lloyd JR. Molecular dynamics study of thermal transport in GaAs-self-assembly monolayer-GaAs junctions with ab initio characterization of thiol-GaAs bonds. J Appl Phys. 2011;109(3):034301.
[50] Liu J, Alhashme M, Yang R. Thermal transport across carbon nanotubes connected by molecular linkers. Carbon. 2012;50(3):1063–70.
[51] Ye Z-Q, Cao B-Y, Guo Z-Y. Study on thermal characteristics of phonons in graphene. Acta Phys Sin. 2014;63:15.
[52] Li Q, Dong Y, Perez D, Martini A, Carpick RW. Speed dependence of atomic stick-slip friction in optimally matched experiments and molecular dynamics simulations. Phys Rev Lett. 2011;106(12):126101.
[53] Fan Y-C, Wu C-D, Fang T-H, Chen T-H. Thermal relaxation and deformation of indented graphene. Comput Mater Sci. 2013;79:105–9.
[54] Zhao L, Cao P. Temperature dependence of contact quality inducing suppression of stick-slip friction. Extreme Mech Lett. 2021;45:101273.